

# Density profile control with current ramping in a transport simulation of IGNITOR

B. Hu<sup>a)</sup> and W. Horton

*Institute for Fusion Studies, The University of Texas at Austin, Austin, Texas 78712*

P. Zhu

*Department of Physics and Astronomy, University of Iowa, Iowa City, Iowa 52242*

F. Porcelli

*Burning Plasma Research Group, INFN and Politecnico di Torino, 10129 Turin, Italy*

(Received 29 August 2002; accepted 2 January 2003)

Current ramping to achieve reversed shear confinement enhancement and peaked density profiles are important for achieving ignition conditions in the high-field tokamak IGNITOR [Coppi *et al.*, Phys. Scri. **45**, 112 (1992)]. Previous transport simulations used either fixed density profiles or obtained flat density profiles leading to a conclusion that a mechanism for peaking the density profile is required for ignition. In this paper an enhanced particle confinement regime that produces ignition before the sawtooth activity begins is explored. It is shown that fast current ramping is a general scheme leading to density profile peaking. In these simulations, peaked density profiles result from the formation of internal transport barrier due to reversed magnetic shear, which is produced by controlled plasma current and volume-averaged density ramping. Such a programmed Ohmic heating scheme is demonstrated to be an effective approach to achieve ignition of a deuterium-tritium plasma. © 2003 American Institute of Physics. [DOI: 10.1063/1.1555623]

## I. INTRODUCTION

Several high performance tokamak operating regimes have been experimentally achieved in experiments through the peaking of density profiles. These include the improved Ohmic confinement regime produced in ASDEX,<sup>1</sup> the pellet enhanced performance mode in the Alcator C tokamak<sup>2</sup> and the Joint European Torus (JET),<sup>3</sup> and the supershot mode in the Tokamak Fusion Test Reactor (TFTR).<sup>4</sup> In these tokamak regimes, the peaked core density profiles bring down the  $\eta_i (= d \ln T_i / d \ln n_i)$  value below the critical threshold for exciting the ion temperature gradient mode, and help to produce internal transport barriers by generating a large sheared radial electric field, which is required for turbulence suppression, through the steep density gradient.<sup>5</sup> In addition to enhancing the confinement, peaked density profiles are also necessary for optimizing the fusion reaction rate and alpha heating power of a tokamak plasma and, when combined with a centrally peaked temperature profile, would help to reach the ignition condition early. Thus, it is desirable to seek and analyze the density profile control schemes that effectively lead to density profile peaking in transport simulations of burning plasma experiments on machines such as IGNITOR.

Previous simulations of IGNITOR experiments either simply utilized density profiles with fixed peaking shape<sup>6</sup> or obtained flat density profiles when self-consistent evolution was allowed.<sup>7</sup> Efforts have been made to increase the core plasma density by pellet injection in IGNITOR simulations;

however, the density profile peaking seems to last for only a short period.<sup>8</sup> Multiple pellet injections would complicate the intrinsically simple Ohmic ignition experiment. In this paper, we demonstrate through transport modeling simulations a scheme for producing peaked density profiles through plasma current ramping, which appears to be an effective method of achieving ignition when sawtooth events are avoided. The basic mechanism is that plasma current ramping at a sufficient rate and with proper timing generates a nonmonotonic  $q$  profile with reversed magnetic shear (RS) during the evolution of the magnetic flux surfaces. An internal transport barrier forms in the reversed shear region which, combined with properly programmed tokamak edge gas puffing, produces a centrally peaked plasma density profile in a timely manner. Since the reversed magnetic shear is a natural by-product of rapid plasma current ramping and also a well-confirmed mechanism in the formation of transport barriers, this type of scheme for density profile peaking is intrinsic to the Ohmic heating process (e.g., used in IGNITOR) and independent of the particular crossfield transport model used in simulations. The modeling does assume that the parallel transport remains neoclassical without anomalous current penetration.

Reversed magnetic shear plasma confinement has become one of the main approaches to achieving fusion-grade plasmas in tokamaks. Reversed magnetic shear confinement has been achieved on several tokamak machines<sup>9-14</sup> and verified from theoretical models.<sup>15,16</sup> An example of using current ramping in an Ohmic tokamak to produce an internal transport barrier (ITB) is the Tore Supra current ramp experiment.<sup>9</sup> In this experiment a high current ramp-up rate defined by  $\omega_{\text{ramp}} = d \ln I_p / dt \sim 10 \text{ s}^{-1}$  is used to create a re-

<sup>a)</sup>Present address: Laboratory for Laser Energetics, University of Rochester, Rochester, NY 14623; electronic mail: bhu@physics.utexas.edu

versed shear plasma, with the current  $I_p$  increasing from 0.4 to 1.2 MA. After the formation of the RS configuration, ion-cyclotron resonance heating power is applied with a time profile that ramps up to 4 MW, starting at the time when  $I_p$  reaches its maximum value of 1.2 MA. In the ensuing steady-state phase, the density is maintained by gas fueling at  $0.65n_G$  [where  $n_G = I(\text{MA})/\pi a^2$  is the Greenwald density limit], and the electron transport barrier is maintained for 2 s. During this 2 s period ( $\geq 50\tau_E$ ) the fluctuation level is reduced and the global energy confinement time is increased by 50%. This scenario is similar to the one used here to reach ignition, except that alpha heating is used in place of the radio-frequency heating.

Here, to demonstrate the scheme, the transport model JETTO<sup>17</sup> is used as a standard model in our simulations with the BALDUR code.<sup>18</sup> JETTO is an empirical model with a mixed Bohm and gyro-Bohm scaling. It has been benchmarked in confinement regimes with and without reversed shear against experimental data from several different tokamak machines.<sup>17</sup> There is no proof that the JETTO model, or any other transport model, can be applied to a compact, high magnetic field Ohmic tokamak. However, the issue of the extrapolation of transport models should not divert our purpose here in an essential way, due to the universal nature of the current ramping scheme.

The rest of the paper is organized as follows. In Sec. II we review the transport model that is used, and describe in detail the simulation scheme. Simulation results are presented and analyzed in Sec. III. Finally in Sec. IV, a summary and discussion are given.

## II. TRANSPORT MODEL AND SIMULATION SCHEME

Here we have adopted the transport model JETTO with reversed shear confinement modes for the simulations of IGNITOR. JETTO is an empirical model containing several extensions to the Taroni–Bohm electron thermal transport model  $\chi_e^B$  originally developed for JET low confinement mode ( $L$ -mode) experiments.<sup>19</sup> Erba *et al.*<sup>20</sup> first extended the Taroni–Bohm model to ion thermal transport  $\chi_i^B$  and to the Ohmic regime. By adding edge temperature gradient dependence, Erba *et al.*<sup>21</sup> further extended their model to  $H$ -mode regimes with transient and nonlocal effects. Later a gyro-Bohm transport term  $\chi_{e,i}^{\text{gB}}$  was included to account for experimental results on other tokamak devices of various sizes.<sup>17</sup> In the normal positive magnetic shear region the standard JETTO model gives the total diffusivities  $\chi_{e,i}$  as the sum of the neoclassical and the anomalous contributions, i.e.,  $\chi_{e,i} = \chi_{e,i}^{\text{neo}} + \chi_{e,i}^A$ . The anomalous thermal diffusivities of electrons and ions take the forms<sup>17</sup>

$$\chi_{e,i}^A = \chi_{e,i}^B + \chi_{e,i}^{\text{gB}} \quad (\text{Bohm term} + \text{gyro-Bohm term}), \quad (1)$$

$$\chi_{e,i}^B = \alpha_{e,i}^B \frac{cT_e}{eB} \frac{q^2 a}{L_{pe}} \langle L_{Te}^* \rangle_{\Delta V}^{-1} \quad (\text{Bohm term}), \quad (2)$$

$$\chi_{e,i}^{\text{gB}} = \alpha_{e,i}^{\text{gB}} \frac{cT_e}{eB} \frac{\rho_{si}}{L_{Te}} \quad (\text{gyro-Bohm term}), \quad (3)$$

independent of the explicit magnetic shear  $s = (r/q)(dq/dr)$ , where  $q$  and  $r$  are the safety factor and the minor radius,

respectively. In Eq. (2)  $\langle L_{Te}^* \rangle_{\Delta V}^{-1} = |(T_e(x=0.8) - T_e(x=1))/T_e(x=1)|$  is the correction factor for nonlocality at the edge;  $L_{pe} = |d \ln p_e/dr|^{-1}$  and  $L_{Te} = |d \ln T_e/dr|^{-1}$  are the electron pressure and electron temperature gradient scale lengths, respectively;  $\rho_{si}$  is the ion Larmor radius at the electron temperature; and the values adopted for the empirical transport coefficients are

$$\alpha_e^B = 8 \times 10^{-5}, \quad \alpha_i^B = 2 \alpha_e^B,$$

$$\alpha_e^{\text{gB}} = 3.5 \times 10^{-2}, \quad \alpha_i^{\text{gB}} = \alpha_e^{\text{gB}}/2,$$

as benchmarked from data in the International Thermonuclear Experimental Research database and the Tore Supra databases.

Weak and reversed magnetic shear has been shown to suppress several dominant magnetohydrodynamic (MHD) instabilities and also microinstabilities in tokamaks, particularly those driven by unfavorable geodesic magnetic curvature.<sup>10,11,22–24</sup> In the present simulations the suppression is given by  $\chi_{e,i} = \chi_{e,i}^{\text{neo}} + \Theta(s+0.1)\chi_{e,i}^A$ , resulting in the formation of an internal transport barrier for  $s < -0.1$ , where the Heaviside step function vanishes for  $s < -0.1$ . In tokamak experiments with transport barriers, reversed shear works either alone or together with some other turbulence suppression mechanism, such as the **E×B** flow shear. This approach of implementing the effects of reversed shear has been adopted in some earlier simulations of internal transport barriers in tokamaks<sup>25</sup> and has been benchmarked in JET. There is supporting theoretical<sup>26</sup> and simulation data for the reduction of anomalous transport by negative magnetic shear. We do not attempt to include the **E×B** shear flow suppression.

The particle diffusivity of the main gas ion species is modeled as

$$D_i = \left[ c_1 + (c_2 - c_1) \frac{r}{a} \right] \frac{\chi_e \chi_i}{\chi_e + \chi_i}, \quad (4)$$

where  $c_1 = 1$  and  $c_2 = 0.3$  are empirical coefficients and  $r/a$  is the normalized minor radius of the device. The form of  $D_i$  arises from taking into account the ambipolar condition  $\Gamma_i = \Gamma_e$  and the approximation  $D_{i,e} \propto \chi_{i,e}$ . The hydrogen ion particle flux  $\Gamma_i$  and heat fluxes  $q_{e,i}$  are calculated from

$$\Gamma_i = -D_i \frac{\partial n_i}{\partial r}, \quad (5)$$

$$q_{e,i} = -n_{e,i} \chi_{e,i} \frac{\partial T_{e,i}}{\partial r}. \quad (6)$$

Formulas (5) and (6) have no critical gradient and give transport for all nonvanishing  $\nabla n_i$  and  $\nabla T_{e,i}$ . There are theoretical and experimental reasons for revising these formulas to include a critical gradient. The electron turbulent transport has shown clear evidence of a critical gradient in the ASDEX<sup>27</sup> and Tore Supra<sup>28</sup> tokamaks. The role of the critical gradient and the associated turbulent particle pinch deserves close examination in future work. A critical gradient term will improve the performance over that reported here.

In our simulations, we choose the global design parameters based on the specifications given in Coppi *et al.*<sup>29</sup> (See

TABLE I. Global parameters for IGNITOR simulations.

Major radius $R$ (m)	Minor radius $a$ (m)	Elongation $\kappa$	Triangularity $\delta$	Toroidal field $B_T$ (T)
1.32	0.47	1.83	0.43	13

Table I.) The relevant initial and boundary conditions for the transport equations are selected as follows. The initial central temperatures for both ions and electrons are set to be 1 keV, and the initial central density is chosen to be  $3.0 \times 10^{20} \text{ m}^{-3}$  for both deuterium and tritium. Initial radial profiles for particle density, temperature, and current density are shown in Sec. III for two simulation runs with fast and slow current ramp rates. During the heating process, the edge temperature increases from 0.3 keV at the beginning to 2.0 keV in the end of the pulse,<sup>7</sup> while the edge density remains at a constant value of  $1.0 \times 10^{20} \text{ m}^{-3}$  for both the deuterium and tritium ion species.

The key procedure of the Ohmic heating scheme in our simulations is the plasma current ramping. The time histories of the plasma current and the volume density for a reference simulation run #ignif01 with peaked density profile are shown in Fig. 1. The plasma current  $I_p$  rapidly increases from its initial value during the first 1.2 s to its maximum value of 12 MA by the end of the ramping stage, then drops to 11 MA and remains there for the rest of the heating process. With a fixed target value of plasma current and a fixed length of ramping period, the average current ramping rate is determined by the initial plasma current. We found that in

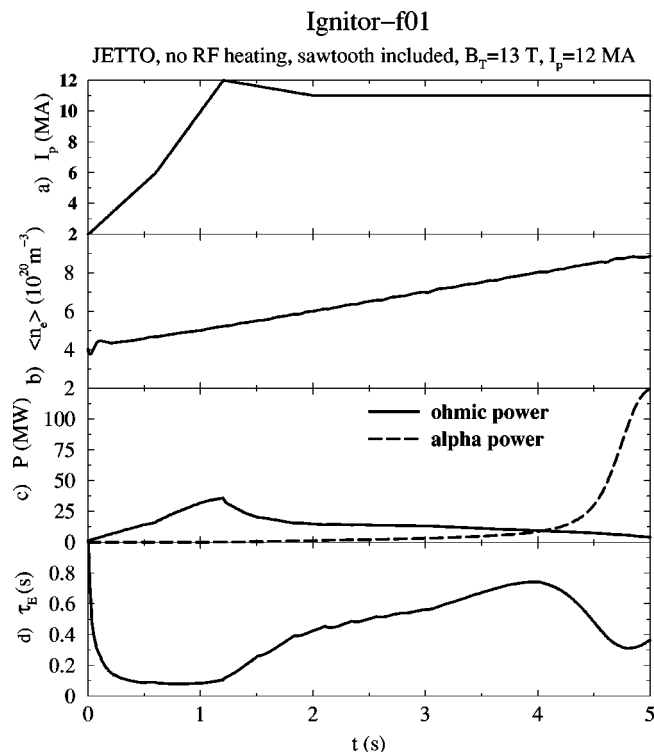


FIG. 1. Time history of (a) plasma current  $I_p$ , (b) volume-average density  $\langle n_e \rangle$ , (c) Ohmic power  $P_{oh}$  and alpha power  $P_\alpha$ , and (d) confinement time  $\tau_E$  in the reference simulation run #ignif01 with a peaked density profile.

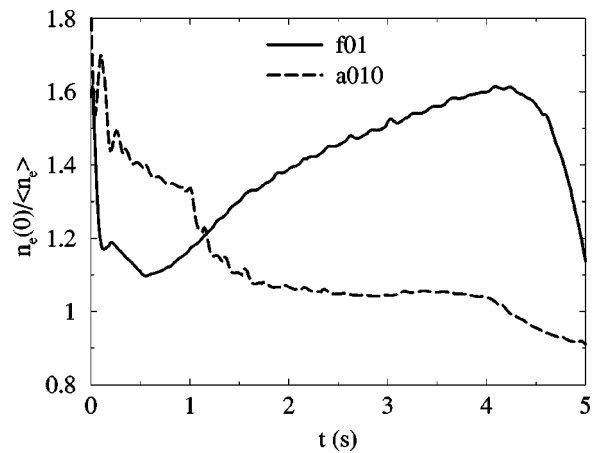


FIG. 2. Comparison of the time evolution of the density profile peakedness  $n_e(0)/\langle n_e \rangle$  for two simulation runs with different current ramping rates.

order to have negative magnetic shear during the time evolution of the magnetic flux surfaces, the initial plasma current should be approximately equal to or less than 4 MA. This corresponds to a threshold for the plasma current ramping rate of approximately 7 MA/s.

The rapid ramping of plasma current is accompanied by a gradual growth of electron volume-average density, starting from  $4.0 \times 10^{20} \text{ m}^{-3}$  and increasing toward its target value of  $9.0 \times 10^{20} \text{ m}^{-3}$ , controlled by neutral gas puffing from the edge (Fig. 1). For a given ramping rate of the plasma current, there is an upper limit for the density ramping rate, above which the desired density profile peaking and plasma ignition would not occur. Our simulation studies show that if the gas fueling rate is too high, the result is that the density peaks near the plasma edge and hence the density profile is hollow. On the other hand, too low a rate of gas fueling would not significantly peak the density profile and thus not raise the central density to the level required for ignition. A staged ramping scheme for volume-averaged density, with the ramping rate carefully chosen between these two extreme limits, ensures the peaking of the density profile and also early ignition, as, for example, in the reference case in Fig. 1.

### III. SIMULATION RESULTS

With the use of the transport model and the simulation scheme described in Sec. II, peaked density profiles were obtained during early time stages (prior to ignition) of the reference simulation run #ignif01. In Fig. 1 we show the optimal current and density ramp that was found. During this time the Ohmic power increases to its maximum of 39 MW, as shown in Fig. 1. The peak of the Ohmic power diminished just at the end of the current ramp. The alpha power was about 40 KW at this time and continued to increase rapidly, as seen in Fig. 1.

Figure 2 shows that the density profile peaking grows in time and the  $q=1$  surface forms late in time. Following Coppi *et al.*,<sup>6</sup> we also use the ratio of the central density to the volume-averaged density  $n_e(0)/\langle n_e \rangle$  as the variable that quantifies the peakedness of the density profile. In Fig. 2, we compare the time evolution of the density profile peakedness

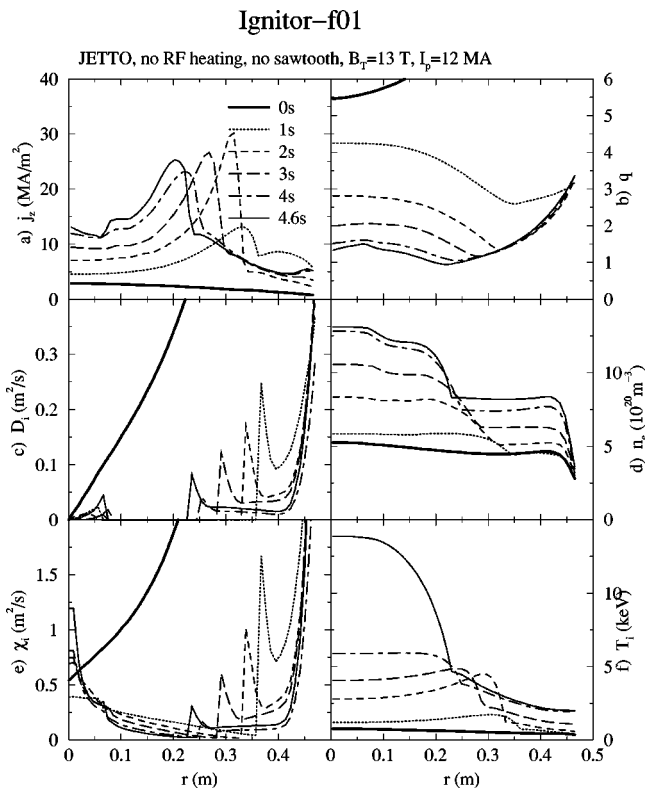


FIG. 3. Radial profiles of (a) plasma current density  $j_z$ , (b) safety factor  $q$ , (c) particle diffusivity  $D_i$ , (d) electron density  $n_e$ , (e) ion thermal conductivity  $\chi_i$ , and (f) ion temperature  $T_i$ , at six time slices  $t=0,1,2,3,4$ , and 4.6 s in the reference simulation run #ignif01.

$n_e(0)/\langle n_e \rangle$  for the two-simulation cases. The correlation between the current ramping rate and the density profile peakedness is apparent for time stages prior to ignition. The radial electron density profiles at six representative time slices are plotted in Fig. 3(d), in comparison with those of corresponding time slices in Fig. 4(d) from an earlier simulation run (#ignia010) with a slower current ramping rate.<sup>7</sup> The peaking of the density radial profile is evident in the reference case #ignif01 prior to ignition, as characterized by an inward moving internal transport barrier.

The peaked density profile seen in our simulations is basically a direct consequence of the formation of an internal transport barrier, produced indirectly by rapid current ramping through reversed magnetic shear. This mechanism for density peaking can be clearly demonstrated by the causal relationships among the time-evolving radial profiles of several transport quantities, including the plasma current density  $j_z$ , the safety factor  $q$ , the particle diffusivity  $D_i$ , the electron density  $n_e$ , the ion thermal conductivity  $\chi_i$ , and the ion temperature  $T_i$  for the reference simulation run #ignif01 in Fig. 3. The initial plasma density and temperature radial profiles spread out but remain flat. During the fast current ramping stage when the poloidal magnetic flux diffuses in from the boundary, most of the plasma current accumulates around the plasma edge if the current ramping rate exceeds the diffusion rate of the magnetic flux. As a result, the safety factor profile  $q(r,t)$  maintains a local minimum between the core and the edge, as does that of the Ohmic heating power depo-

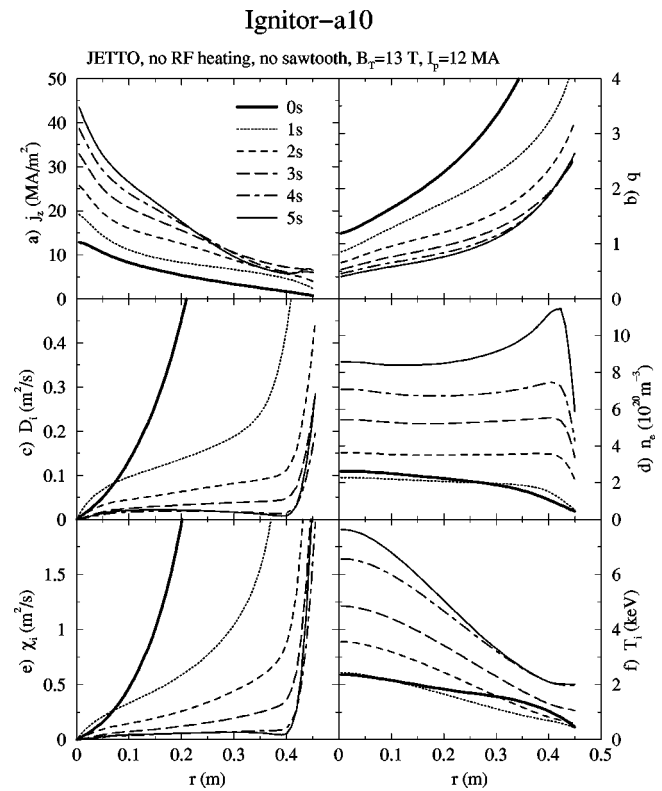


FIG. 4. Radial profiles of (a) plasma current density  $j_z$ , (b) safety factor  $q$ , (c) particle diffusivity  $D_i$ , (d) electron density  $n_e$ , (e) ion thermal conductivity  $\chi_i$ , and (f) ion temperature  $T_i$ , at six time slices  $t=0,1,2,3,4$ , and 5 s in the reference simulation run #ignia010.

sition. The reversed magnetic shear leads to the suppression of both particle and thermal transport in that region, forming steep gradients in both density and temperature profiles there, namely, an internal transport barrier. As the plasma is heated up, the reversed shear region and the transport barrier both slowly move inward, resulting in the peaking of the density profile. The timing and location of the reversed shear region and the transport barrier are well correlated in the radial profiles shown in Fig. 3. As a comparison, the corresponding process in the earlier slow current ramp simulation run #ignia010 is shown in Fig. 4, where neither the RS region nor the ITB is present.

The favorable effects of density profile peaking on ignition were demonstrated earlier by Coppi *et al.*<sup>6</sup> However, our studies here differ from those of Coppi *et al.* in that the peaked density profile in our transport simulations is produced dynamically by plasma current ramping, instead of being prescribed by a fixed density profile as in Coppi *et al.* As shown here, a plasma with a peaked density profile during the heating process can reach ignition before a sawtooth is triggered, which ensures ignition.

In Fig. 5 we compare the time traces of the alpha-heating power  $P_\alpha$  and the total confinement power loss  $P_L$  for the simulation runs shown in Fig. 2 with two different levels of density profile peaking due to different plasma current ramping rates. Ignition, defined as the condition when the alpha-heating power  $P_\alpha$  is balanced by the total thermal loss  $P_L$ , can be seen to occur at  $t=4.24$  s in simulation #ignif01 with

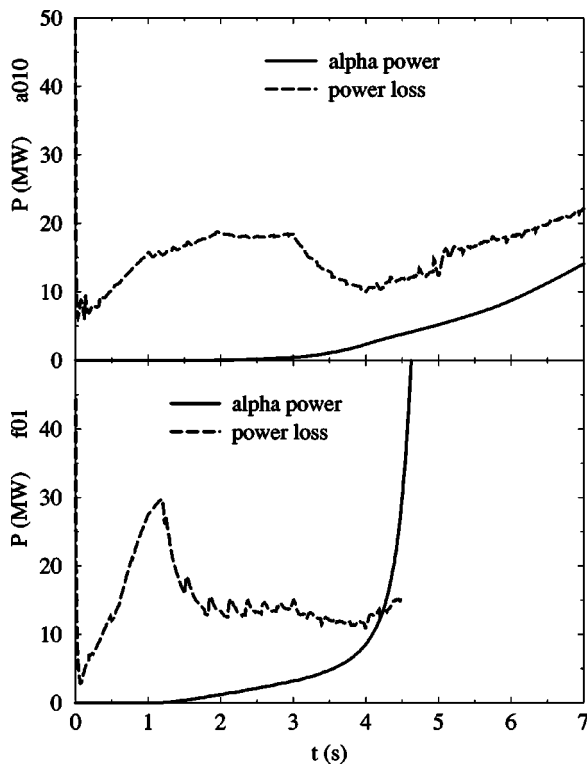


FIG. 5. Time traces of alpha-heating power  $P_\alpha$  and the total confinement power loss  $P_L$  in the two simulation runs shown in Fig. 2.

density profile peaking, whereas the  $q=1$  surface is born at  $t=4.34$  s in the middle of the minor radius. In simulation runs with a lower current ramping rate, sawtooth events begin earlier than the time when the ignition conditions are met, which may prevent ignition from occurring.

The density rise in the center of the plasma due to edge neutral gas puffing is explained as follows. In the boundary layer of the plasma, the neutrals interact with the electrons and the ions through two separate processes: ionization and charge exchange. Recombination in the plasma is negligible. Because of the ionization due to electron-neutral interactions, the neutrals with velocity  $v_n$  can only penetrate a certain distance

$$\lambda_n = \frac{v_n}{n_e \langle \sigma_{\text{ion}} v_e \rangle}. \quad (7)$$

In the case of IGNITOR, for 2 keV electron temperature, the ionization rate is about  $10^{-14} \text{ m}^3 \text{ s}^{-1}$ . At the edge of the IGNITOR plasma, the electron density is about  $2 \times 10^{20} \text{ m}^{-3}$ , and the penetration length  $\lambda_n$  for 2 keV neutrals is about 0.3 m, which is smaller, although comparable to, the minor radius  $a=0.47$  m of IGNITOR. In the core region, the electrons have a much higher temperature and density, and the actual penetration length for the neutrals is smaller than the minor radius of IGNITOR.

In the reversed shear confinement simulation for IGNITOR with the BALDUR code, the neutral density  $n_{\text{neu}}$  at the core region is maintained at approximately  $10^{12} \text{ m}^{-3}$ , three orders of magnitude lower than that at the edge of the plasma. However, with a high ionization rate  $\langle \sigma_{\text{ion}} v_e \rangle$ , whose value is about  $10^{-14} \text{ m}^3 \text{ s}^{-1}$  in the temperature range

$10-10^4$  eV, the source term from the ionization process is approximately  $n_{\text{neu}} n_e \langle \sigma_{\text{ion}} v_e \rangle \sim 6 \times 10^{19} \text{ m}^{-3} \text{ s}^{-1}$ , large enough to significantly raise the electron and ion densities in the core region.

The other atomic process is charge exchange, i.e., an energetic plasma hydrogen ion captures an electron from a lower-energy neutral. This process is particularly important for hydrogen, because the rate is greater than that for ionization. The penetration of neutrals is largely influenced by charge exchange. There is not much energy exchanged by the charge-exchange collision, since the emerging neutral has nearly the same energy as the incident plasma ion. For a plasma temperature of 10–100 eV, this cross section  $\sigma_{\text{cx}}$  is approximately  $4 \times 10^{-19} \text{ m}^2$ , which is nearly two orders of magnitude larger than the ionization cross section. For a plasma with  $T_e \approx T_i$ , the charge-exchange rate is usually two-to-three times larger than the ionization rate. The charge-exchange cross section is large because it is a resonant effect, in which the initial and the final quantum states almost have no energy difference. For the 2 keV ion temperature in the IGNITOR simulation case, the charge-exchange rate  $\langle \sigma_{\text{cx}} v_i \rangle$  is about  $10^{-13} \text{ m}^3 \text{ s}^{-1}$ . When low-energy neutrals are injected into the edge of a plasma, charge exchange will increase the penetration of neutrals into the hot dense plasma by producing a second generation of energetic neutrals with kinetic energies comparable to the multi-keV ions. As time goes on, the interaction between the second generation neutrals and the inner more energetic ions will produce third-generation neutrals and so on.

The BALDUR code includes these processes through the use of Monte Carlo calculations of the neutral atom transport and ionization. The neutral particle package in BALDUR was benchmarked with TFTR data.<sup>30</sup>

#### IV. SUMMARY

The simulations reported in this paper demonstrate a scheme for obtaining a peaked density profile during the heating process of IGNITOR through the formation of an internal transport barrier by rapid plasma current ramping. At the initial stage of Ohmic heating, the plasma current density accumulates in the outer region if the ramping rate of the total plasma current exceeds its inward diffusion rate. A minimum point in the profile of the safety factor  $q$  appears where the plasma current density accumulates, forming a region with reversed magnetic shear. An internal transport barrier is thus produced in that region, due to the suppression of the fluctuations by reversed and weak magnetic shear there. Following the inward movement of the transport barrier as the plasma current diffuses farther inside, a peaked density and a peaked temperature profile are obtained. Peaked density and temperature profiles that result from the transport barrier enable the plasma to reach ignition conditions before the occurrence of sawtooth events, and hence ensure the achievement of ignition. Although the JETTO transport model is used in our simulations, this type of density profile peaking scheme is in principle independent of the particular choice of transport model, since it derives from the intrinsic feature of Ohmic heating and current diffusion processes in

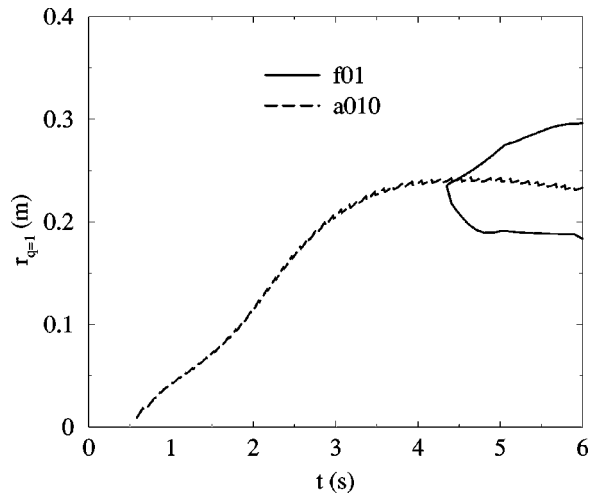


FIG. 6. Time traces of the position of the  $q=1$  surface for cases a010 and f01.

the IGNITOR experiment and from the universal mechanism of transport barrier formation due to reversed magnetic shear. In particular, we used the standard multimode transport model<sup>30</sup> and still obtained similar reversed shear  $q$  profiles and density peaking effect. Purely theoretical models of  $\mathbf{E} \times \mathbf{B}$  transport with reversed shear also show reduced transport.<sup>16</sup>

The nonmonotonic  $q$  profiles may also delay the onset of sawteeth. Figure 6 shows the time evolution of the radial position of the  $q=1$  surface. For the slow current ramping case a010, the  $q \leq 1$  region appears very early from the center of the plasma and quickly extends to the middle of the radius. For the fast current ramping case f01, the  $q \leq 1$  region is born at midradius at a much later time than in case a010, and the  $q \leq 1$  region has a smaller volume than in a010. Sawtooth activity is more likely to be easily controlled in the f01 fast current ramp case than in the a010 slow current ramp case.

Nonmonotonic current density profiles may lead to MHD instabilities, e.g., resistive interchange and double-tearing modes. A previous study<sup>31</sup> indicated that the nonlinear evolution of double-tearing modes would lead to anomalously fast current penetration. Clearly, this is an undesirable result for IGNITOR, because it would prevent magnetic shear reversal and the formation of an internal transport barrier. On the other hand, recent experience, especially in tokamaks investigating advanced confinement scenarios, indicates that nonmonotonic  $q$  profiles can be sustained at least transiently, i.e., for time scales that are relatively short compared with the global resistive diffusion time. This would be sufficient for the successful operation of IGNITOR with reversed shear. In the absence of conclusive theoretical evidence, it would be desirable to test the IGNITOR-relevant reversed shear scenarios in existing tokamak experiments, such as CMOD,<sup>32</sup> the Frascati Tokamak Upgrade (FTU),<sup>33</sup> and DIII-D,<sup>34</sup> where high-density, high-field plasma conditions can be realized. In our simulation studies, we have tried the fast current ramping scenario for CMOD and Tore Supra. For the CMOD case, we did not obtain reversed shear with a

3 MA/s current ramping rate. For the Tore Supra case, we did obtain reversed shear with the published current ramping rate of 1.6 MA/s.<sup>9</sup> The resistive time for current diffusion is  $\tau_{cd} \sim \mu_0 a^2 / \eta$ . The minor radius is  $a = 0.21, 0.27, 0.63, 0.8$  m, for CMOD, FTU, DIII-D, and Tore Supra, respectively. The resistivity  $\eta$  for the same electron temperature does not vary much for different tokamak machines. The only important factor is  $a^2$ . The minor radius of DIII-D is comparable to that of Tore Supra; thus it should be possible to achieve reversed shear on DIII-D in a pure ohmic heating discharge with a viable current ramping rate. This scenario is expected to be difficult for FTU and very difficult for CMOD. In fact, we tried a series of fast current ramps on CMOD and barely obtained reversed shear with a current ramping rate of 9 MA/s, compared to the reference value of 3 MA/s. Currently, we are investigating the possibility of achieving reversed shear with rf heating to raise the electron temperature prior to the current ramping.

In conclusion, the use of programmed current ramps and density ramps in a transient high-field tokamak burning plasma experiment may allow ignition to be achieved without the complication of rf heating and pellet injection. Simulations with critical gradients giving offset-linear electron fluxes<sup>27,28,35,36</sup> are suggested as future studies.

## ACKNOWLEDGMENTS

We acknowledge useful discussions with J. Callen, G. Bateman, G. Hallock, A. Kritz, L. Sugiyama, F. Bombarda, and B. Coppi.

This work was supported by the Engineering Research Program of the Office of Basic Energy Science at the U.S. Department of Energy through Grant No. DE-FG03-96ER-54346.

<sup>1</sup>F. X. Söldner, E. R. Müller, F. Wagner, H. S. Bosch, A. Eberhagen, H. U. Fahrbach, G. Fussmann, O. Gehre, K. Gentle, J. Gernhardt *et al.*, Phys. Rev. Lett. **61**, 1105 (1988).

<sup>2</sup>M. J. Greenwald, D. A. Gwinn, S. Milora *et al.*, Phys. Rev. Lett. **53**, 352 (1984).

<sup>3</sup>P. H. Rebut, R. J. Bickerton, and B. E. Keen, Nucl. Fusion **25**, 1011 (1985).

<sup>4</sup>R. J. Hawryluk *et al.*, in *Plasma Physics and Controlled Nuclear Fusion Research, Proceedings of the 11th International Conference, Kyoto, Japan, 1986* (International Atomic Energy Agency, Vienna, 1987), Vol. 1, p. 51.

<sup>5</sup>T. S. Hahm, Plasma Phys. Controlled Fusion **44**, A87 (2002).

<sup>6</sup>B. Coppi, M. Nassi, and L. E. Sugiyama, Phys. Scr. **45**, 112 (1992).

<sup>7</sup>W. Horton, F. Porcelli, P. Zhu, A. Aydemir, Y. Kishimoto, and T. Tajima, Nucl. Fusion **42**, 169 (2002).

<sup>8</sup>C. N. Nguyen and G. Bateman (private communication).

<sup>9</sup>G. T. Hoang, C. Bourdelle, X. Garbet, G. Antar, R. V. Budny, T. Aniel, V. Basiuk, A. Becoulet, P. Devynck, J. Lasalle *et al.*, Phys. Rev. Lett. **84**, 4593 (2000).

<sup>10</sup>F. Levinton, M. Zarnstorff, S. Batha, M. Bell, R. Bell, R. Budny, C. Bush, Z. Chang, E. Fredrickson, A. Janos *et al.*, Phys. Rev. Lett. **75**, 4417 (1995).

<sup>11</sup>E. Strait, L. Lao, M. Mauel, B. W. Rice, T. S. Taylor, K. H. Burrell, M. S. Chu, E. A. Lazarus, T. H. Osborne, S. J. Thompson *et al.*, Phys. Rev. Lett. **75**, 4421 (1995).

<sup>12</sup>S. Ishida, T. Fujita, H. Akasaka, N. Akino *et al.*, Phys. Rev. Lett. **79**, 3917 (1997).

<sup>13</sup>C. Gormezano, Y. F. Baranov, C. D. Challis, I. Coffey *et al.*, Phys. Rev. Lett. **80**, 5544 (1998).

<sup>14</sup>S. Günter, R. C. Wolf, F. Leuterer, O. Gruber *et al.*, Phys. Rev. Lett. **84**, 3097 (2000).

- <sup>15</sup>W. Horton, H.-B. Park, J. M. Kwon, D. Strozzi, P. J. Morrison, and D.-I. Choi, *Phys. Plasmas* **5**, 3910 (1998).
- <sup>16</sup>J. M. Kwon, W. Horton, P. Zhu, P. J. Morrison, H.-B. Park, and D.-I. Choi, *Phys. Plasmas* **7**, 1169 (2000).
- <sup>17</sup>M. Erba, T. Aniel, V. Basiuk, E. Becoulet, and X. Litaudon, *Nucl. Fusion* **38**, 1013 (1998).
- <sup>18</sup>C. E. Singer *et al.*, *Comput. Phys. Commun.* **49**, 275 (1988).
- <sup>19</sup>A. Taroni, M. Erba, E. Springmann, and F. Tibone, *Plasma Phys. Controlled Fusion* **36**, 1629 (1994).
- <sup>20</sup>M. Erba, V. Parail, E. Springmann, and A. Taroni, *Plasma Phys. Controlled Fusion* **37**, 1249 (1995).
- <sup>21</sup>M. Erba, A. Cherubini, V. Parail, E. Springmann, and A. Taroni, *Plasma Phys. Controlled Fusion* **39**, 261 (1997).
- <sup>22</sup>C. Kessel, J. Manickam, G. Rewoldt, and W. M. Tang, *Phys. Rev. Lett.* **72**, 1212 (1994).
- <sup>23</sup>M. A. Beer, G. W. Hammett, G. Rewoldt, E. J. Synakowski, M. C. Zarnstorff, and W. Dorland, *Phys. Plasmas* **4**, 1792 (1997).
- <sup>24</sup>Y. Kishimoto, J.-Y. Kim, W. Horton, T. Tajima, M. J. LeBrun, and H. Shirai, *Plasma Phys. Controlled Fusion* **41**, A663 (1999).
- <sup>25</sup>V. Parail, Y. Baranov, C. Challis, G. Cottrell, B. Fischer, C. Gormezano, G. Huysmans, X. Litaudon, A. Sips, F. Sldner *et al.*, *Nucl. Fusion* **39**, 429 (1999).
- <sup>26</sup>P. Zhu, G. Bateman, A. H. Kritz, and W. Horton, *Phys. Plasmas* **7**, 2898 (2000).
- <sup>27</sup>F. Rytter, F. Leuterer, G. Pereverzev, H.-U. Fahrback, J. Stober, W. Suttrop, and ASDEX Upgrade Team, *Phys. Rev. Lett.* **86**, 2325 (2001).
- <sup>28</sup>G. T. Hoang, C. Bourdelle, X. Garbet, G. Giruzzi, T. Aniel, M. Ottaviani, W. Horton, P. Zhu, and R. V. Budny, *Phys. Rev. Lett.* **87**, 125001 (2001).
- <sup>29</sup>B. Coppi, A. Airoidi, F. Bombarda, G. Cenacchi, P. Detragiache, C. Ferro, R. Maggiora, L. Sugiyama, and G. Vecchi, Report PTP 99/06, MIT (RLE) (September 1999), in Ref. 7.
- <sup>30</sup>G. Bateman, A. H. Kritz, J. E. Kinsey, A. J. Redd, and J. Weiland, *Phys. Plasmas* **5**, 1793 (1998).
- <sup>31</sup>B. Carreras, H. R. Hicks, and B. V. Waddell, *Nucl. Fusion* **19**, 583 (1979).
- <sup>32</sup>I. H. Hutchinson, R. Boivin, F. Bombarda *et al.*, *Phys. Plasmas* **1**, 1511 (1994).
- <sup>33</sup>R. Cesario, C. Castaldo, V. Pericoli-Ridolfini *et al.*, in *Proceedings of the 13th Topical Conference on Radio Frequency Power in Plasmas, 1999 Annapolis, MD*, edited by S. Bernabei and F. Paoletti (American Institute of Physics, New York, 1999), p. 100.
- <sup>34</sup>J. Luxon *et al.*, in *Plasma Physics and Controlled Nuclear Fusion Research, Proceedings of the 11th International Conference, Kyoto, Japan, 1986* (International Atomic Energy Agency, Vienna, 1987), Vol. 1, p. 159.
- <sup>35</sup>H. Sugama, M. Okamoto, W. Horton, and M. Wakatani, *Phys. Plasmas* **3**, 2379 (1996).
- <sup>36</sup>B. Coppi and C. Spight, *Phys. Rev. Lett.* **41**, 551 (1978).